

# Detecting Primordial Stars

Evan Scannapieco<sup>1</sup>, Andrea Ferrara<sup>2</sup>, Alexander Heger<sup>3</sup>  
Piero Madau<sup>4</sup>, Raffaella Schneider<sup>5</sup>, & Stan Woosley<sup>4</sup>

<sup>1</sup>*Kavli Institute for Theoretical Physics, UC Santa Barbara, CA 93106*

<sup>2</sup>*SISSA/Int. School for Advanced Studies, Via Beirut 4, 34014 Trieste, Italy*

<sup>3</sup>*Theoretical Astrophysics Group, T6, MS B227, Los Alamos National Laboratory,  
Los Alamos, NM, 87545*

<sup>4</sup>*Dept. of Astronomy & Astrophysics, UC Santa Cruz, Santa Cruz, CA, 95064*

<sup>5</sup>*Osservatorio Astrofisico di Arcetri, Largo E. Fermi 5, 50125 Firenze, Italy*

---

## Abstract

We study the detectability of primordial metal-free stars, both through direct searches for their emission, as well as searches for the resulting supernovae. We show that enrichment is a local process that takes place over an extended redshift range. While the duration of the transition from a metal-free to an enriched universe depends on several unknown factors, in all models late-forming metal-free stars are found in  $10^{7.5} M_{\odot} - 10^{8.0} M_{\odot}$  objects, which are just large enough to cool within a Hubble time, but small enough to not be clustered near areas of previous star formation. We discuss the observational properties of these objects, some of which may have already been detected in ongoing surveys of high-redshift Lyman- $\alpha$  emitters.

If metal-free stars have masses  $140 M_{\odot} \lesssim M_{\star} \lesssim 260 M_{\odot}$ , they are expected to end their lives as pair-production supernovae (PPSNe), in which an electron-positron pair-production instability triggers explosive nuclear burning. Using the implicit hydrodynamics code KEPLER, we calculate a set of PPSNe light curves that allows us to assess observational strategies for finding these objects. The peak luminosities of typical PPSNe are only slightly greater than those of Type Ia supernovae, but they remain bright much longer ( $\sim 1$  year) and have hydrogen lines. Ongoing supernova searches may soon be able to place stringent limits on the fraction of very massive stars out to  $z \approx 2$ . The planned *Joint Dark Energy Mission* satellite will be able to extend these limits out to  $z \approx 6$ .

*Key words:* cosmology, theory, galaxy formation, supernovae

---

## 1 Introduction

A long time ago there were no metals. The primordial fireball generated a whirlwind of neutrinos, an ocean of thermal photons, and a mountain of light nuclei, but failed to produce elements heavier than lithium. In fact, it was not until several hundred million years later that the universe was first enriched with heavy elements.

Yet, today stellar nucleosynthetic products are everywhere. The lowest metallicity galaxies known are enriched to substantial values of  $\sim 0.02Z_\odot$  (1); the lowest-density regions of the intergalactic medium (IGM) appear to be enriched out to the highest redshifts probed (2; 3; 4); and although direct observations of metal-poor halo stars have uncovered a number of unusual abundance patterns (5; 6), not a single metal-free star has ever been detected.

Thus a clear signature of the transition from a metal-free to an enriched universe has so far remained unobserved. Furthermore, there are good reasons to believe that this transition may have marked a drastic change in the characteristics of stars. Recent theoretical studies have shown that collapsing primordial clouds fragmented into clumps with typical masses  $\sim 10^3 M_\odot$  (7; 8; 9; 10) and that accretion onto proto-stellar cores within these clouds was very efficient (12; 13). The implication is that the initial mass function (IMF) of primordial stars may have been biased to higher masses than observed today.

## 2 The Epoch of Metal-Free Stars

The work discussed in this section and in §3 is described in further detail in (11). As the detailed shape of the metal-free IMF is highly uncertain, we adopted a wide range of theoretical models that are based on studies of primordial gas cooling and fragmentation (7; 8; 9; 10). In these investigations, the minimum fragment mass was comparable to the Jeans mass at the temperature and density at which molecular hydrogen levels start to be populated according to LTE, which is  $\sim 10^3 M_\odot$ .

With these studies in mind, we parameterized the IMF with a range of models in which the IMF is a Gaussian of the form  $\frac{1}{\sqrt{2\pi}\sigma_C} e^{-(M-M_C)^2/2\sigma_C^2}$ , where  $100 M_\odot \leq M_C \leq 1000 M_\odot$  and  $\sigma_C^{\min} \leq \sigma_C \leq \sigma_C^{\max}$ . Finally, we also explored a “null hypothesis” in which the distribution of metal-free stars is given by a Salpeter IMF. These models can be parameterized in turn by a single quantity,  $E_g^{III}$  the “energy input per unit gas mass,” which is the product of the fraction of gas mass that goes into stars ( $f_\star$ ), the number of supernovae per  $M_\odot$  of stars ( $N_{SN}^{III}$ ), the kinetic energy input per SN in units of  $10^{51}$  ergs ( $E_{SN}^{III}$ ),

and the fraction of the SN kinetic energy that gets channeled into an outflow, dispersing the metals ( $f_w$ ) outside the host galaxy. Thus  $E_g^{III} = f_* N_{SN}^{III} E_{SN}^{III} f_w$  has units of  $10^{51}$  ergs  $M_\odot^{-1}$ .

Zero-metallicity stars with initial masses  $140 M_\odot \lesssim M_* \lesssim 260 M_\odot$  are expected to end their lives as pair-production supernovae PPSNe, in which an electron-positron pair-production instability triggers explosive nuclear burning (14; 15). In this case, the kinetic energy per SN is  $\approx 50 \times 10^{51}$  ergs, and the ejected metal mass is  $\approx 100 M_\odot$  (15). In conventional core-collapse supernovae, the energy per SN is about  $10^{51}$  ergs and roughly  $2 M_\odot$  of metal are ejected. Thus regardless of the IMF, the total mass in metals is roughly  $2 M_\odot$  per  $10^{51}$  ergs of kinetic energy input.

In other words, despite the many uncertainties surrounding metal-free stars, the total energy in each outflow and the total metal mass dispersed are closely related. Using a simple 1-D outflow model (16) to study the metallicity evolution within each dispersal event, we have found that for the full range of parameters considered, the mean metallicity of outflows from primordial objects is well above the critical threshold ( $Z_{cr} \sim 10^{-4} Z_\odot$ ) that marks the formation of normal stars (10). This means that primordial star formation continued well past the time at which the average IGM metallicity reached  $Z_{cr}$ , as large areas of the IGM remained pristine while others were enriched to many times this value. Enrichment was a local process, and the history of metal-free formation is likely to have been determined almost exclusively by the efficiency of metal ejection, parameterized by  $E_g^{III}$ .

To track the dispersal of the first ejected metals, we made use of the analytical formalism described in (17) [see also (18)] coupled with our 1-D outflow model. The resulting evolution of the star formation rate (SFR) density and the mean cosmic metallicity are shown in Figure 1. Here  $E_g^{III}$  ranges from the  $10^{-4}$  value appropriate for a Salpeter IMF to the extreme  $10^{-2.5}$  value appropriate for an IMF composed almost solely of  $\sim 200 M_\odot$  stars.

In all models, while the peak of primordial star formation occurs at  $z \sim 10$ , such stars continue to contribute appreciably to the SFR density at much lower redshifts. This is true even though the mean IGM metallicity has moved well past the critical transition metallicity. Furthermore, for many models, substantial primordial star formation continues well into the observable redshift range, contributing to as much as 10% of the SFR at  $z = 5$ . In all cases these objects tend to be in the  $10^{7.5} M_\odot - 10^{8.0} M_\odot$  mass range, just large enough to cool within a Hubble time, but small enough that they are not clustered near areas of previous star formation.

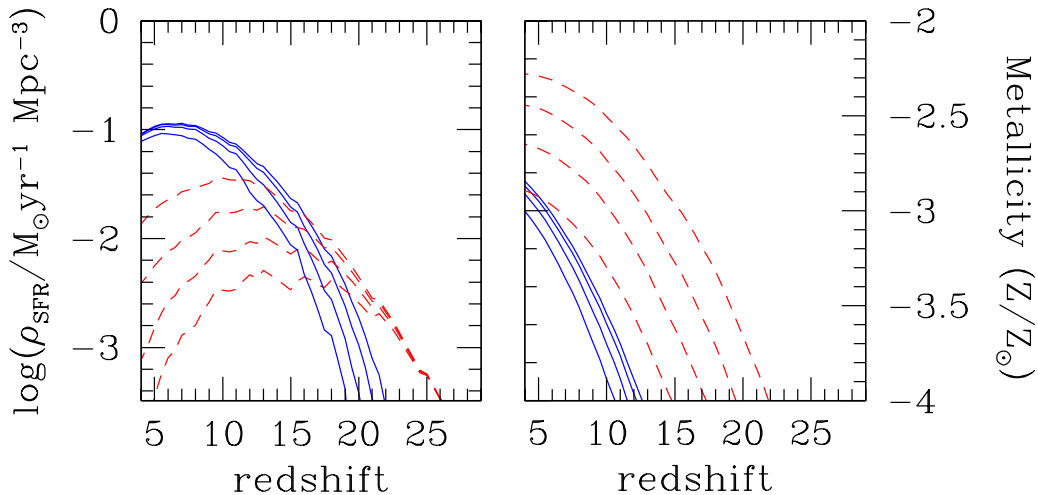


Fig. 1. Star formation rate densities for primordial and PopII/I objects. All models assume  $f_{\star}^{III} = 0.1$ ,  $f_{\star}^{II} = 0.1$ , and  $f_w = 0.1$ . *Left* : SFR density per cubic comoving Mpc for primordial objects (dashed lines) and PopII/I objects (solid lines). We consider models in which, from top to bottom,  $\log_{10}(E_g^{III}) = -4.0$   $-3.5$ ,  $-3.0$ , and  $-2.5$ . *Right*: IGM average metallicity resulting from primordial (dashed lines) and PopII/I (solid lines) objects. Again,  $\log_{10}(E_g^{III})$  ranges from  $-4.0$  to  $-2.5$  from top to bottom.

### 3 Direct Detections of Primordial Objects

Employing a simple model of burst-mode star formation, we have developed a rough characterization of these directly observable primordial objects. As metal-free stars are powerful Ly $\alpha$  line emitters (19; 20), it is natural to use this indicator as a first step in any search for primordial objects. The Ly $\alpha$  luminosity,  $L_{\alpha}$ , is directly related to the corresponding hydrogen ionizing photon rate,  $Q(H)$ , by  $L_{\alpha} = c_L(1 - f_{\text{esc}})Q(H)$ , where  $c_L \equiv 1.04 \times 10^{-11}$  erg and  $f_{\text{esc}}$  is the escape fraction of ionizing photons from the galaxy. For this uncertain factor we adopt an educated guess of  $f_{\text{esc}} = 0.2$ , which is based on a compilation of theoretical and observational results (21). We compute  $Q(H)$  from evolutionary stellar models: either from STARBURST99 (22) in the Salpeter IMF case, or from the models in (20) in the case of very massive stars.

In Figure 2 the isocontours in the Ly $\alpha$  luminosity-redshift plane indicate the probability to find a galaxy hosting metal-free stars in a given sample of emitters, again for various values of  $E_g^{III}$ . In the left panel of Figure 2, we consider a model in which metal-free stars form according to a Salpeter IMF. Although in this case the Ly $\alpha$  emission from these stars is slightly brighter than from their PopII/I counterparts (19), this difference is not dramatic. However, as outflows are relatively weak ( $E_g^{III} \sim 10^{-4}$ ), and thus  $\sim 10\%$  of  $z = 5$  Ly $\alpha$  emitters with observed fluxes above  $1.5 \times 10^{-17}$  ergs cm $^{-2}$  s $^{-1}$  are likely be

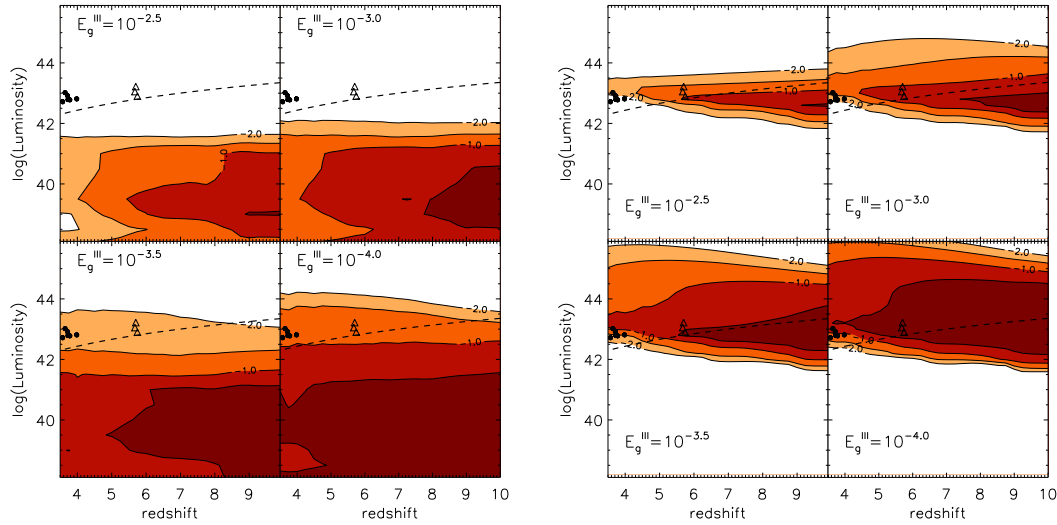


Fig. 2. Fraction of primordial objects as a function of Ly $\alpha$  luminosity and redshift. Isocontours of fractions  $\geq 10^{-2}$ ,  $10^{-1.5}$ ,  $10^{-1}$ , and  $10^{-0.5}$  are shown. The left panels correspond to a model with a Salpeter IMF, while the right panels correspond to a model in which primordial stars are  $\sim 200 M_{\odot}$ . Each panel is labeled by its assumed  $E_g^{III}$  value. For reference, the dashed line gives the luminosity corresponding to an observed flux of  $1.5 \times 10^{-17}$  ergs  $\text{cm}^{-2} \text{s}^{-1}$ , and the points correspond to a number of recent measurements [See (11) for details].

made up of metal-free stars.

In the right panel of Figure 2, we consider a model in which the metal-free IMF is peaked at  $\sim 200 M_{\odot}$ . In this case the short but bright evolution of such stars boosts their luminosities by over an order of magnitude. However, the ejection of the resulting metals is dramatically more efficient ( $E_g^{III} \sim 10^{-3}$ ), and thus again  $\sim 10\%$  of  $z = 5$  Ly $\alpha$  emitters are metal-free.

Thus it is likely that a number of metal-free objects are lurking at the limit of present surveys. The goal then is to find a clear-cut feature that uniquely identifies a given object as metal-free. The most simple such criterion is the equivalent width of Ly $\alpha$ , which should be higher in primordial stars than in a normal population, as such stars burn hotter and generate more ionizing photons (19), particularly in the very-massive case (20). In fact, such large equivalent widths have indeed been seen in the observed populations of high-redshifts Ly $\alpha$  emitters (23), although this can also be the result of other mechanisms, such as scattering in a clumpy, dusty medium (24).

A much less ambiguous indicator has been identified by (25), who noted that primordial stars produce large He III regions, which may emit detectable He II recombination emission. The recombination lines at  $\lambda 1640 \text{ \AA}$  ( $n = 3 \rightarrow 2$ ),  $\lambda 3203 \text{ \AA}$  ( $n = 5 \rightarrow 3$ ), and  $\lambda 4686 \text{ \AA}$  ( $n = 4 \rightarrow 3$ ) are particularly attractive for this purpose because they suffer minimal effects of scattering by gas and

decreasing attenuation by intervening dust. For star formation rates of  $20 M_{\odot} \text{ yr}^{-1}$  and  $5 M_{\odot} \text{ yr}^{-1}$  in a given galaxy, the  $\lambda 1640$  flux is detectable out to  $z \approx 5$  at the sensitivity level of current surveys, although the flux for  $\lambda 4686$  is 7.1 times lower. While these lines also arise from Wolf-Rayet stars, they would be accompanied by strong metal lines in this case (27). Metal-free stars, on the other hand, are uniquely intense sources of pure He-II emission. Note that this spectroscopic test is particularly difficult, however, as metal-free stars should only be found in a small fraction of  $z = 5$  objects, and composite spectra are likely to wipe out such a signal. Thus the observed absence of the 1640 doublet in the combined spectra from the *Large Area Lyman Alpha* survey (28) is consistent with all but the most optimistic of the models in Fig 2.

#### 4 Pair-Production Supernovae

The work discussed in this section is described in further detail in (26). If primordial stars were indeed very massive, the resulting pair-production supernovae may be directly detectable. This approach has the advantage of constraining the total rate density of very massive star formation as a function of redshift, regardless of how they are distributed in galaxies of different sizes.

Previously, only very limited or approximate models of PPSNe have been available in the literature (29; 30; 31; 32). Here we use the KEPLER code (33) to directly construct a suite of PPSN lightcurves that addresses the range of theoretical possibilities and accounts for the detailed physical processes involved up until the point at which the SN becomes optically thin. These results are shown in Figure 3.

For most of their lifetimes, the effective temperatures of PPSNe are just above the  $\approx 10^{3.8} K$  recombination temperature of hydrogen, which corresponds to a peak black-body wavelength  $\approx 8000 \text{ \AA}$ . The most important factors in determining the features in the luminosity evolution of these SNe are the mass of the progenitor star and the efficiency of dredge-up of carbon from the core into the envelope. In general, increasing the mass leads to greater  $^{56}\text{Ni}$  production, which boosts the late time SN luminosity, through radioactive decay. Mixing, on the other hand, has two major effects: it increases the opacity in the envelope, leading to a red giant phase that increases the early-time luminosity; and it decreases the mass of the He core, consequently decreasing the  $^{56}\text{Ni}$  mass and lowering the late-time luminosity.

Despite these uncertain factors, PPSNe in general can be characterized as SNe that have all three key features: (1) peak magnitudes that are brighter than Type II SNe and comparable or slightly brighter than typical SNe Type Ia; (2) very long decay times  $\approx 1$  year, which result from the large initial radii

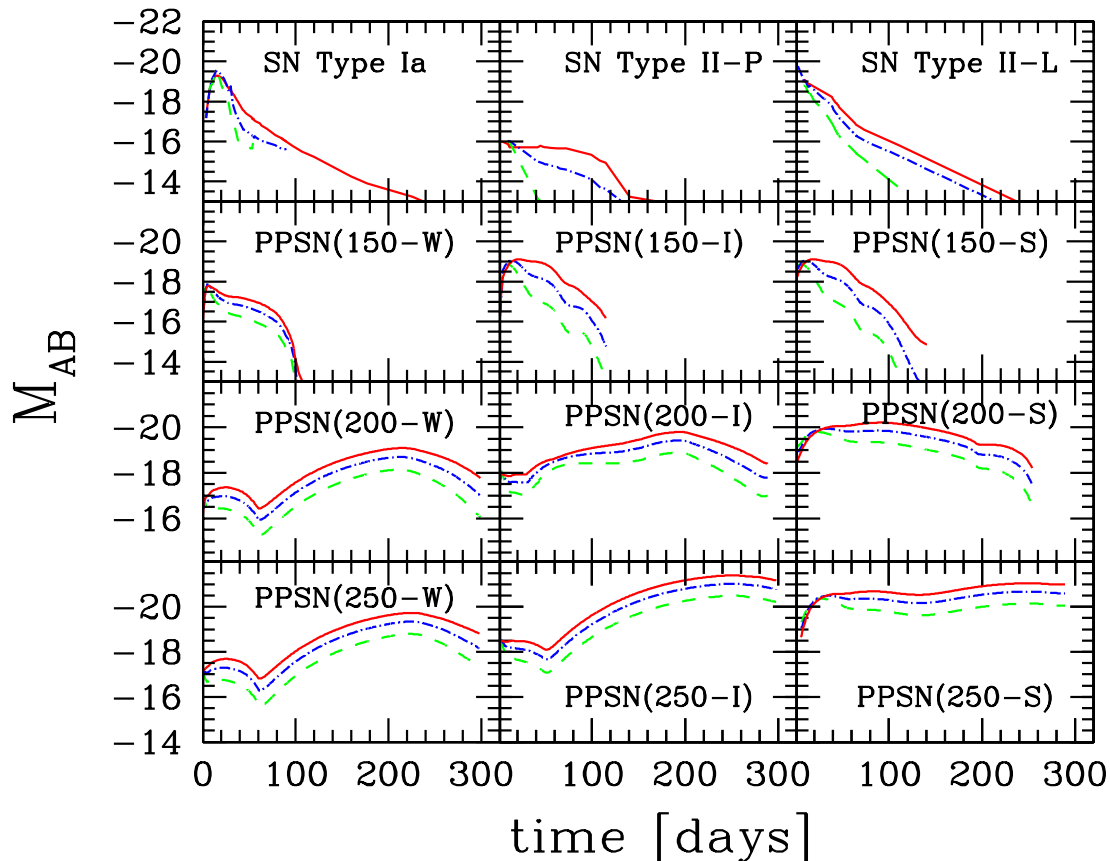


Fig. 3. Comparison of light curves of a SN Type Ia, a SN Type II-P, a bright SN Type II-L, and PPSNe models with varying progenitor masses. In all cases the solid lines are absolute V-band AB magnitudes, the dot-dashed lines are the absolute B-band AB magnitudes, and the dashed lines are the absolute U-band AB magnitudes. The model names refer to the mass of the progenitor star (in units of  $M_{\odot}$ ) and the weak (W), intermediate (I), or strong (S) level of mixing by convective overshoot.

and large masses of material involved in the explosion; and (3) the presence of hydrogen lines, which are caused by the outer envelope. Note, however, that only this last feature is present in *all* cases, and in fact, the lowest mass PPSNe models we constructed have lightcurves that are remarkably similar to those of SN Type II.

Accounting for redshifting, time dilation, and appropriate luminosity factors, we used these lightcurves to relate the overall very massive SFR density to the number of PPSNe detectable in current and planned supernova searches. As the metal-free SFR density is unknown, we adopted two simple models, which can be easily shifted for comparison with literature models, including our models in Fig. 1. In the first model, we assume that metal-free star formation occurs at a constant rate density, which we take to be  $10^{-3} M_{\odot} \text{ yr}^{-1} \text{ Mpc}^{-3}$ , independent of redshift. In the second case, we assume that at all redshifts

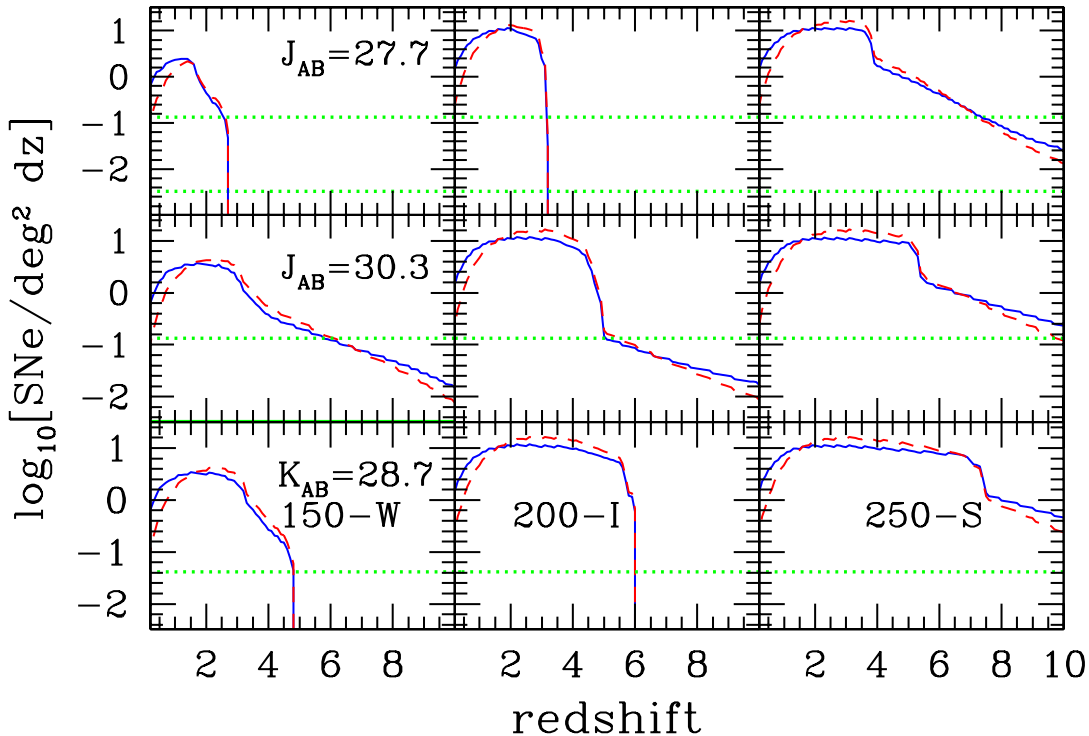


Fig. 4. Number of PPSNe per square degree per unit redshift above a fixed broad-band magnitude, assuming  $0.001 \text{ M}_{\odot} \text{ yr}^{-1} \text{ Mpc}^{-3}$  (solid lines) or 1% of the observed SFR density (dashed lines). *Top*: The  $J_{\text{AB}} = 27.7$  limit taken in these panels corresponds to a single scan in the planned deep-field *SNAP* survey, which would cover  $7.5 \text{ deg}^2$  (indicated by the upper dotted lines). A similar magnitude limit with the same coverage would be obtained with 2 months of grism data from the *Destiny* mission. The full planned  $700 \text{ deg}^2$  wide-field *SNAP* survey (lower dotted lines) also has the same limiting magnitude. *Center*: The  $J_{\text{AB}} = 30.3$  limit taken in these panels is that of the deep-field *SNAP* survey, which would be able to place constraints on PPSN out to  $z \gtrsim 5$ . *Bottom*: Curves corresponding to the *JEDI* mission, with a magnitude limit of  $K_{\text{AB}} = 28.7$  and a coverage of over  $24 \text{ deg}^2$  with 2 months of data. At the highest redshifts, this search does substantially better than the fainter, but bluer  $J_{\text{AB}} = 30.3$ , search. This is because at these redshifts the peak of the PPSNe spectra is shifted to  $\approx 40000 \text{ \AA}$ , and observations at longer wavelengths represent an exponential increase in the observed flux.

metal-free stars form at 1% of the observed total SFR density, which we model with a simple fit to the most recent measurements (34; 35). In all cases we assume that  $N_{\text{SN}}^{\text{III}}$ , the number PPSNe per  $\text{M}_{\odot}$  of stars formed, is  $10^{-3}$ .

Comparing these models with ongoing surveys, we find that significant limits on PPSNe can already be placed out to moderate redshifts. Given the area and magnitude limit of the the *Institute for Astronomy Deep Survey* (36), for example, one can constrain very massive star formation to  $\lesssim 1\%$  of the total



SFR density out to a redshift of 2.

Future missions should improve these limits greatly. In Fig. 4, we show the PPSN constraints that would be obtained from three possible realizations of the planned space-based *Joint Dark Energy Mission (JDEM)*. In the upper panel we adopt a limit of  $J_{AB} = 27.7$ , corresponding to the wide-field survey planned for the *Supernova Acceleration Cosmology Probe (SNAP)*<sup>1</sup> realization of *JDEM*. With 2 months of data, the alternative *Dark Energy Space Telescope (Destiny)*<sup>2</sup> realization of *JDEM* would cover 7.5 deg<sup>2</sup> of sky with spectroscopic observations down to a similar limit. In the central panel, we take a limit of  $J_{AB} = 30.3$  which would correspond to the deep-field *SNAP* survey. In the lower panel, we consider a redder survey with a limiting magnitude of  $K_{AB} = 28.7$ , as appropriate for two months of observations from the *Joint Efficient Dark-energy Investigation (JEDI)*<sup>3</sup> realization of *JDEM*.

Although planned with completely different goals in mind, these supernova searches will also serve as fantastic probes of PPSNe. Depending on the realization, *JDEM* may be able to place stringent limits on the rate density of even the faintest PPSNe out to  $z \approx 4$ . For more luminous models, PPSNe will be constrained out to  $z \approx 6$  and beyond. Thus, while a definitive measurement of metal-free stars remains allusive, narrow-band, spectroscopic, and SNe searches are fast closing in on these objects. The future of primordial star detection looks bright.

I would like to thank UC Irvine and the organizing committee for hosting this enjoyable and informative workshop.

## References

- [1] L. C. Searle and W. L. W. Sargent, *ApJ*, **173**, 25 (1972)
- [2] J. Schaye et al., *ApJ*, **596**, 768 (2003)
- [3] B. Aracil, P. Petitjean, C. Pichon, and J. Bergeron, *A&A*, **419**, 811 (2004)
- [4] M. Pettini et al., *ApJ*, **594**, 695 (2003)
- [5] N. Christlieb et al., *Nature*, **419**, 904 (2002)
- [6] R. Cayrel et al., *A&A*, **416**, 1117 (2004)
- [7] F. Nakamura and M. Umemura, *ApJ*, **515**, 239, (1999)
- [8] T. Abel, G. Bryan, and M. Norman, *ApJ*, **540**, 39, (2000)
- [9] V. Bromm, A. Ferrara, P. S. Coppi P, and R. B. Larson, *MNRAS*, **328**, 969 (2001)

---

<sup>1</sup> see <http://snap.lbl.gov/>

<sup>2</sup> see <http://destiny.asu.edu/>

<sup>3</sup> see <http://jedi.nhn.ou.edu/>

- [10] R. Schneider, A. Ferrara, P. Natarajan, and K. Omukai, *ApJ*, **571**, 30 (2002)
- [11] E. Scannapieco, R. Schneider, and A. Ferrara, *ApJ*, **589**, 35 (2003)
- [12] E. Ripamonti, F. Haardt, A. Ferrara, and M. Colpi, *MNRAS*, **334**, 401 (2002)
- [13] J. C. Tan and C. F. McKee, *ApJ*, **603**, 383 (2004)
- [14] J. R. Bond, W. D. Arnett, and B. J. Carr, *ApJ*, **280**, 825 (1984)
- [15] A. Heger and S. E. Woosley, *ApJ*, **567**, 532 (2002)
- [16] J. P. Ostriker and C. F. McKee, *Rev. Mod. Phys.*, **60**, 1 (1988)
- [17] E. Scannapieco and R. Barkana, *ApJ*, **571**, 585 (2002)
- [18] C. Porciani, S. Matarrese, F. Lucchin, and P. Catelan, *MNRAS*, **298**, 1097 (1998)
- [19] J. Tumlinson, J., J. M. Shull, and A. Venkatesan, *ApJ*, **584**, 608 (2003)
- [20] D. Schaerer, *A&A*, **382**, 28 (2002)
- [21] R. Ciardi, S. Bianchi, and A. Ferrara, *MNRAS*, **331**, 463 (2002)
- [22] L. Leitherer et al., *ApJS*, **123**, 3 (1999)
- [23] S. Malhotra, and J. E. Rhoads, *ApJ*, **565**, L71 (2002)
- [24] M. Hansen, this volume
- [25] J. Tumlinson, J., M. Giroux, and J. M. Shull, *ApJ*, **555**, 839 (2001)
- [26] E. Scannapieco, P. Madau, S. E. Woosley, A. Heger, and A. Ferrara, preprint [arXiv:astro-ph/0507182]
- [27] D. C. Abbott and P. S. Conti, *ARA&A*, **25**, 113 (1987)
- [28] S. Dawson et al., *ApJ*, **617**, 707 (2002)
- [29] S. E. Woosley and T. A. Weaver NATO ASIC Proc. 90: Supernovae: A Survey of Current Research, 79 (1982)
- [30] K. Herzig, M. F. El Eid, K. J. Fricke, and N. Langer, *A&A*, **233**, 462 (1990)
- [31] A. Heger, S. E. Woosley, I. Baraffe, and T. Abel 2002, in “Lighthouses of the Universe: The Most Luminous Celestial Objects and Their Use for Cosmology,” *Proc. of the MPA/ESO*, p. 369 (2002) [arXiv: astro-ph/0112059]
- [32] J. H. Wise and T. Abel [arXiv: astro-ph/0411558]
- [33] T. A. Weaver, G. B. Zimmerman, G. B., and S. E. Woosley, *ApJ*, **225**, 1021 (1978)
- [34] Giavalisco et al., *ApJ*, **600**, L103 (2004)
- [35] Bouwens et al., *ApJ*, **616**, L79 (2004)
- [36] B. J. Barris et al., *ApJ*, **602**, 571 (2004)